

# Analysis of electro-optical intensity modulator for bunch arrival-time monitor at SXFEL

Jin-Guo Wang<sup>1,2</sup> · Xiao-Qing Liu<sup>1</sup> · Lie Feng<sup>1</sup> · Wen-Yan Zhang<sup>1</sup> · Xing-Tao Wang<sup>1</sup> · Bo Liu<sup>1</sup>

Received: 4 July 2018 / Revised: 14 August 2018 / Accepted: 1 October 2018 / Published online: 2 January 2019  
© China Science Publishing & Media Ltd. (Science Press), Shanghai Institute of Applied Physics, the Chinese Academy of Sciences, Chinese Nuclear Society and Springer Nature Singapore Pte Ltd. 2019

**Abstract** A bunch arrival-time monitor (BAM) based on an electro-optical intensity modulation scheme is currently under development at Shanghai Soft X-ray Free-Electron Laser to meet the high-resolution requirements for bunch stability. The BAM uses a radio frequency signal generated by a pickup cavity to modulate the reference laser pulses in an electro-optical intensity modulator (EOM), and the bunch arrival-time information is derived from the amplitude change of the laser pulse after laser pulse modulation. EOM is a key optical component in the BAM system. Through the basic principle analysis of BAM, many parameters of the EOM are observed to affect the measurement resolution of the BAM system. Therefore, a systematic analysis of the EOM is crucial. In this paper, we present two schemes to compare and analyze an EOM and provide a reference for selecting a new version of the EOM.

**Keywords** Bunch arrival-time monitor (BAM) · Soft X-ray Free-Electron Laser (SXFEL) · High resolution · Electro-optical intensity modulator (EOM)

## 1 Introduction

X-ray free-electron lasers (XFELs) [1–6] with fully coherent, high-intensity, and ultrashort pulses can be an effective tool to study the structure and dynamic process of matter on the atomic scale, thereby pushing the frontiers in different disciplines, such as physics, chemistry, and material science [7, 8]. In order to provide a stable operation of the FEL in pump–probe experiments and seeded schemes (such as high gain harmonic generation (HG), echo-enabled harmonic generation (EEHG), and two-stage cascade) [9–14], the arrival-time of electron bunches must be controlled with femtosecond accuracy. Therefore, a high-precision measurement of the bunch arrival time is crucial for the synchronization process.

Currently, at the Shanghai Soft X-ray Free-Electron Laser (SXFEL) [15], a bunch arrival-time monitor (BAM) based on an electro-optical intensity modulation scheme [16–18] is under development. This BAM has the potential to achieve sub-10-femtosecond resolution. The radio frequency (RF) signal induced by the electromagnetic field of the electron bunch modulates the laser pulse train propagated from the synchronization system in a Mach–Zehnder-type electro-optical intensity modulator (EOM). The modulated laser pulse carries the arrival-time information of the electron bunch. A laser pulse is phase-shifted to the RF signal zero-crossing point, and this moment's RF signal is determined as a benchmark signal. The degree of the subsequent modulated laser pulse offset relative to the zero-crossing position is the relative time information of the electron bunch. The degree of this offset is proportional to the amplitude of the modulated laser pulses.

---

This work was supported by the National Key R&D Plan (No. 2016YFA0401900).

✉ Bo Liu  
liubo@sinap.ac.cn

<sup>1</sup> Shanghai Institute of Applied Physics, Chinese Academy of Science, Shanghai 201204, China

<sup>2</sup> University of the Chinese Academy of Science, Beijing 100049, China

The bunch arrival-time information is derived from the amplitude change of the laser pulse after laser pulse modulation. The reason for choosing the zero-crossing point as the reference point is that the slope of the RF signal zero-crossing point is the largest. Furthermore, it is a linear area near the zero-crossing point, which can be used to measure the time information of whether the bunch is advanced or delayed. Because this modulation process is performed in the EOM, many parameters of the EOM will affect this modulation efficiency, and this efficiency needs to be considered when analyzing the resolution of the BAM system to achieve maximum BAM resolution. A detailed analysis of the parameters that affect the resolution of the BAM system by EOM is necessary to provide guidance for the optimization of the next generation of BAM system.

In this paper, we first present the basic principle of the BAM system and a theoretical derivation of the electro-optical intensity modulation in the EOM. The remainder of this paper describes the design of two different schemes to study an EOM in the same test environment and a comparative analysis of the results.

## 2 Principle of BAM

A schematic diagram of the bunch arrival-time monitor is shown in Fig. 1. The BAM system is mainly composed of three parts: the RF front end, the electro-optical modulation front end, and the readout electronics.

The electromagnetic field excited by the electron bunch will induce the RF signal at the pickup pole of the pickup

cavity, which is a high-bandwidth, bipolar RF signal. In order to increase the peak-to-peak value of the RF, a combiner combines two symmetry extraction poles of the pickup cavity and connects them to the RF modulation port of an EOM via a phase stable coaxial cable. The EOM RF port often has a maximum voltage limit; thus, a limiter must be added to the EOM RF port to protect the EOM from being damaged. The electro-optical modulation front end is the center of the BAM system, where the laser pulses are modulated by the RF signal.

The laser pulse train generated from the synchronization system enters the chassis of the electro-optical modulation front-end system and passes an optical delay line (ODL). The ODL has a 560 ps optical delay range. It is used to scan the RF signal and shift the laser pulse signal to the zero point of the RF signal. After the ODL, the laser pulses are divided into two channels by an optical splitter: One of the signals is transmitted to the EOM, and the other is used as a sampling clock for the analog-to-digital converter (ADC) to synchronize with the laser pulse from the EOM channel. The EOM is the core of the electro-optical-modulation front end as the arrival-time information of bunches is transferred there. In the EOM, the RF signal coming from the RF front end modulates the laser pulse divided by the optical splitter. The amplitude of the laser pulse will change with its relative position to the RF signal. The modulated laser pulses are transmitted out of the tunnel to the readout electronics for subsequent signal acquisition, processing, and analysis.

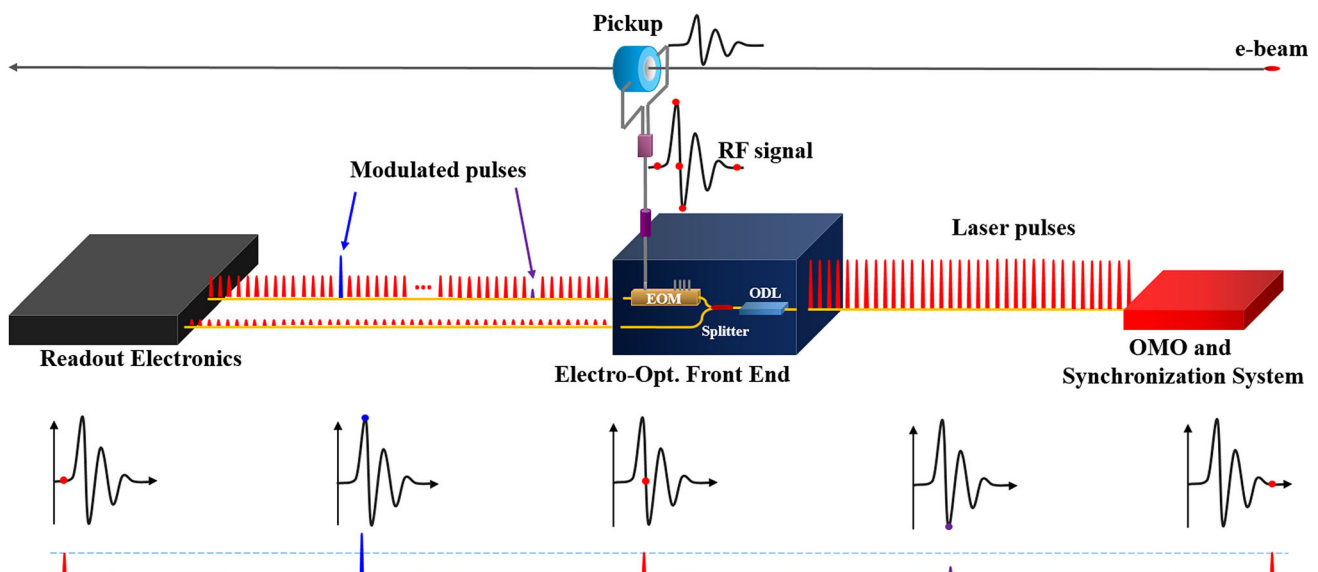


**Fig. 1** (Color online) Schematic of bunch arrival-time monitor. Different positions of laser reference pulses relative to the pickup signal are displayed at different modulation amplitudes

### 3 Theoretical description

As an optical device, the EOM is a Mach–Zehnder electro-optical intensity modulator used in BAM. A basic principle diagram of the EOM is shown in Fig. 2, and the transmission of light intensity modulation signals is shown in Fig. 3.

When the laser pulse enters the EOM, it splits into two symmetrical light branches through a 3-dB directional coupler. The electric field applied by the external electrode modulates the refractive index of the two optical paths and thus introduces a phase shift after the two laser pulses propagate into two branches. Furthermore, the refractive index is a function of the strength of the electric field. When the two laser pulses are recombined at the output, their phase shift change will be converted into a laser pulse amplitude modulation. According to [19, 20], the transfer function of an intensity modulator can be described as

$$I_O = T_r \times I_i \times \left[ \frac{1}{2} + \frac{1}{2} \cos \left( \frac{\pi \times U_{bias}(t)}{V_{\pi,bias}} + \frac{\pi \times U_{RF}(t)}{V_{\pi,RF}} + \emptyset \right) \right], \tag{1}$$

where  $I_O$  and  $I_i$  are the output and input power intensity of the laser, respectively.  $T_r$  is the modulation depth of the EOM optical transmission. The intrinsic initial phase term of the EOM is presented by  $\emptyset$ . This phase term  $\emptyset$  is from a small difference between the two optical paths owing to material inhomogeneity and manufacturing tolerances.  $V_{\pi,bias}$  and  $V_{\pi,RF}$ , which are also intrinsic parameters, are the half-wave voltages of the EOM. The static operating point of the EOM is set by  $U_{bias}$ .  $U_{RF}$  represents the pickup signal from the RF front end. The Quad operating modulation point without the pickup signal is determined by  $U_{bias}$  as

$$I_{Quad} = T_r \times I_i \times \left[ \frac{1}{2} + \frac{1}{2} \cos \left( \frac{\pi \times V_{Quad}}{V_{\pi,bias}} + \emptyset \right) \right] = \frac{T_r \times I_i}{2}, \tag{2}$$

where  $\cos \left( \frac{\pi \times V_{Quad}}{V_{\pi,bias}} + \emptyset \right) = 0$ .

Modulation  $I_M$  based on the pickup signal is calculated by

$$I_M = I_O - I_{Quad} = \frac{1}{2} \cos \left( \frac{\pi \times V_{Quad}}{V_{\pi,bias}} + \emptyset + \frac{\pi \times U_{RF}(t)}{V_{\pi,RF}} \right) = \frac{T_r \times I_i}{2} \sin \left( \frac{\pi \times U_{RF}(t)}{V_{\pi,RF}} \right). \tag{3}$$

Normalized modulation  $M$  is described by

$$M = \frac{I_M}{I_i} = \frac{T_r}{2} \sin \left( \frac{\pi \times U_{RF}(t)}{V_{\pi,RF}} \right), \tag{4}$$

and  $U_{RF}(t) = \frac{V_{\pi,RF}}{\pi} \arcsin \left( 2 \times \frac{M}{T_r} \right)$ .

The slope  $S$  of the zero-crossing position near the pickup signal can be approximated as linear in a short interval [21]:

$$U_{RF}(t) \approx S \times t. \tag{5}$$

where  $t$  is the time offset of the laser pulse relative to the zero-point position of the pickup signal. Thus,  $t$  can be represented as

$$t = \frac{V_{\pi,RF}}{S \times \pi} \arcsin \left( 2 \times \frac{M}{T_r} \right). \tag{6}$$

According to the Taylor series expansion of  $\arcsin(2 \times M)$ ,  $t$  can be expressed as

$$t \approx \frac{V_{\pi,RF}}{S \times \pi} \left[ \left( 2 \times \frac{M}{T_r} \right) + \frac{\left( 2 \times \frac{M}{T_r} \right)^3}{(3)!} + \frac{\left( 2 \times \frac{M}{T_r} \right)^5}{(5)!} \dots \frac{\left( 2 \times \frac{M}{T_r} \right)^{(2 \times n + 1)}}{(2 \times n + 1)!} \right]. \tag{7}$$

The measurement resolution of the arrival-time information of the bunch will be affected by the amplitude noise of the laser pulse  $\Delta M$ . For the first term of the Taylor series

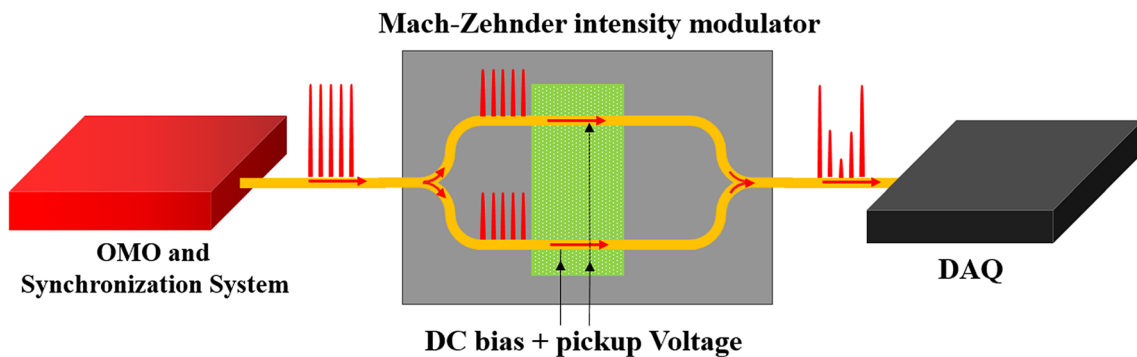
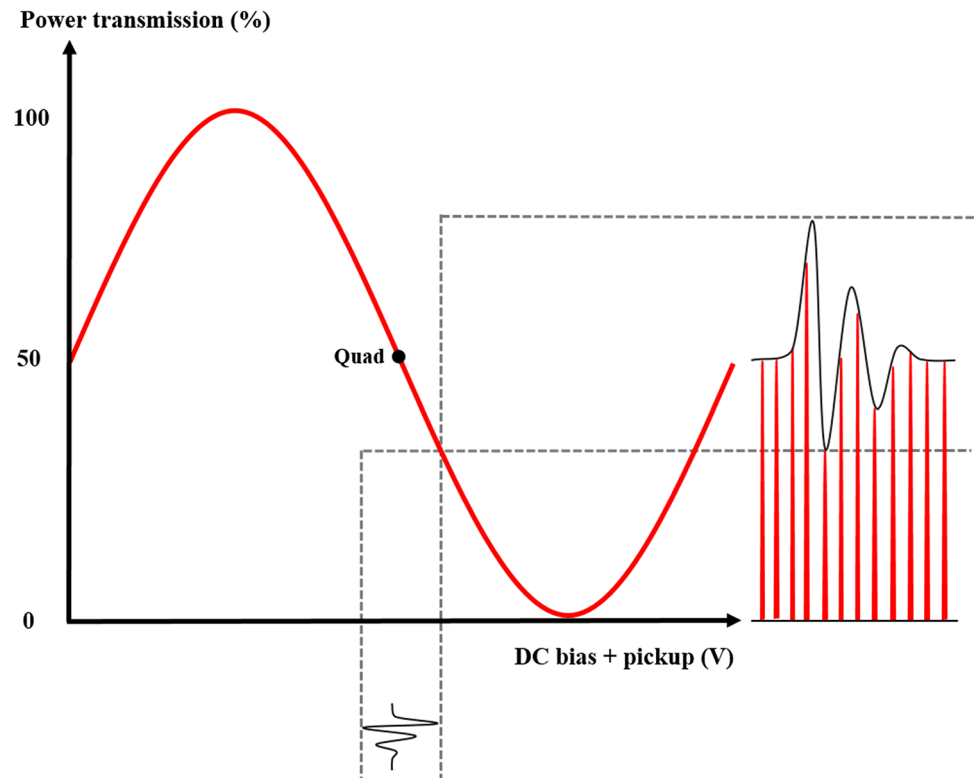


Fig. 2 (Color online) Mach–Zehnder electro-optical intensity modulator

**Fig. 3** (Color online)  
Transmission of light intensity  
modulation signals



in Eq. (7), the bunch arrival-time measurement resolution  $\Delta t$  can be estimated as follows:

$$\Delta t \approx \frac{2 \times V_{\pi,RF}}{S \times \pi \times T_r} \times \Delta M. \quad (8)$$

Therefore, we can observe from Eq. (8) that  $V_{\pi,RF}$  and  $T_r$  are determined by the inherent properties of the EOM device. A lower  $V_{\pi,RF}$  and a larger  $T_r$  are desirable. Similarly, a reasonable value of  $V_{Quad}$  is also very important because it is related to the thermal power of the entire EOM device.

#### 4 EOM performance measurement

The commercially available EOM in the marketplace is mainly used in the telecommunications field. Different from its application in the telecommunications field, a laser pulse train is provided to the EOM. Therefore, it is necessary to verify the fitness between the laser pulse train and the EOM. Nowadays, a LiNbO<sub>3</sub>-type commercial EOM is used in the BAM system. The key parameters of this EOM from the official datasheet are as follows (Table 1) [22].

**Table 1** Key parameters from official datasheet

Supplier	Material	Bandwidth	$V_{\pi,bias}$	$V_{\pi,RF}$ @ 10 GHz
Photline	LiNbO <sub>3</sub>	12 GHz	6.5 V	6.5 V

Based on the symmetry of the internal structure of the EOM,  $V_{\pi,bias}$  can be used to describe  $V_{\pi,RF}$ . Therefore, stepwise scanning of the DC bias voltage is performed through the DC bias port, and the overall performance of the EOM is described by the measured transmission curve.

In order to verify whether the key parameters of EOM in the input of the laser pulse are consistent with the official datasheet used as telecommunications application, two test platforms are set up.

##### 4.1 Test platform based on optical power meter

For a comparison verification, a high-sensitivity optical power meter-based measurement scheme was proposed. The block diagram of the test platform is shown in Fig. 4.

The tested laser pulse train is provided directly by the optical synchronization system. The input laser pulse power can be adjusted by an optical power attenuator placed in front of the EOM. Stepwise scanning of the voltage is added to the EOM's DC bias port. The scan voltage is increased from  $-10$  to  $+10$  V at 0.07-V intervals. Through a full stepwise scanning, an EOM laser pulse transmission curve for the bias voltage was obtained and is shown in Fig. 5.

According to the operating principle of the BAM, the measured transmission curve is analyzed. Many parameters have been drawn for the DC bias voltage, which is related to the selection of the reference operation point. Based on

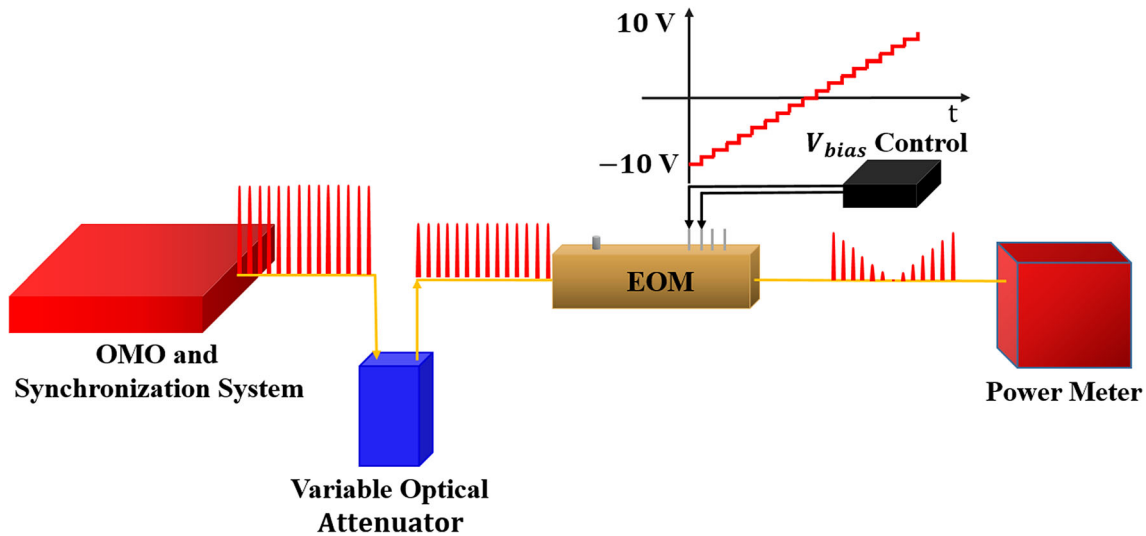


Fig. 4 (Color online) Block diagram of test platform based on optical power meter

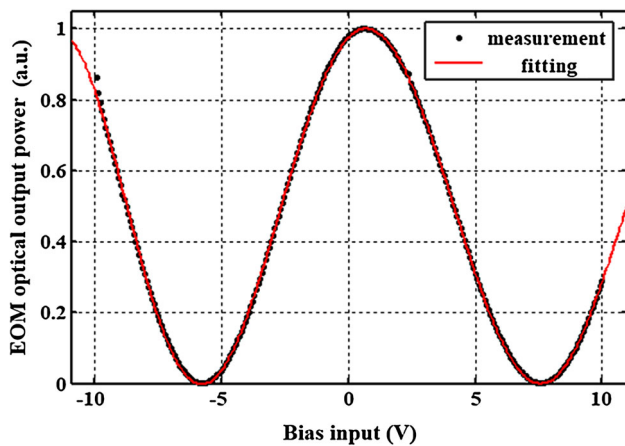


Fig. 5 (Color online) Dependence of EOM laser pulse output power on voltage applied to DC bias port measured by optical power meter

the measured transmission curve, the half-wave voltage value of  $V_{\pi, \text{bias}}$  is determined to be 6.44 V. For this particular EOM, an operation point voltage of Quad point = - 2.68 V is applied at around 50% of the transmission curve (marked with red dots in Fig. 6). A linear region (marked with a pink line in Fig. 6) between 20 and 80% of the transmission curve is typically selected as the modulation region to prevent excessive modulation voltages from bringing the modulation into the nonlinear region. The linearity of this region is calculated by  $R^2 = 0.9996$ . By Eq. (8), the modulation depth  $T_r$  is an important parameter, which is determined with  $T_r = 0.999$  from Fig. 7.

### 4.2 Test platform based on DAQ system

The EOM is an optical integrated circuit that is very sensitive to temperature. Therefore, it is necessary to periodically correct the operating voltage of the EOM for different environments (especially the temperature). This is a real-time performance that cannot be achieved by the optical power meter. As shown in Fig. 8, a test platform based on a Data Acquisition (DAQ) system can realize real-time measurement and determine a new operating point to correct. A DAQ system principle block diagram is shown in Fig. 9.

The basic principle of the DAQ system is to use a homologous laser pulse as the ADC clock signal to sample the peak of the electrical pulse signal after photoelectric conversion, and the transmission curve of the laser pulse is obtained after a full DC bias voltage scan. Based on the measured transmission curve, the half-wave voltage value of  $V_{\pi, \text{bias}}$  is determined to be 6.38 V, and the operation position value of the Quad position = - 2.53 V. The linearity of the region from 20 to 80% is calculated by  $R^2 = 0.9991$ .

As shown in Fig. 10, the bottom of the transmission curve is distorted near the voltages - 6 V or + 8 V. After a photodiode, the laser pulse signal is converted into a bipolar electrical pulse signal. Since the used ADC board is an AC input, it prevents offsetting of the electrical pulse signal by the DC bias voltage. Therefore, when the laser pulse power is very weak, the negative half-axis value of the electrical pulse signal cannot be collected, and distortion is caused.

**Fig. 6** (Color online) Based on optical power meter  $V_{\pi,bias}$ , Quad point voltage and linearity of a linear region  $R^2$  can be measured and calculated

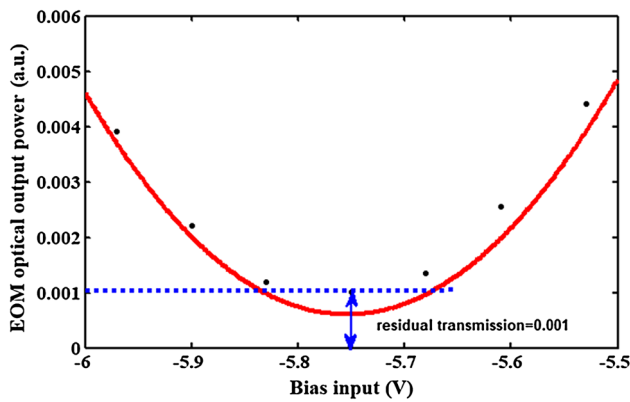
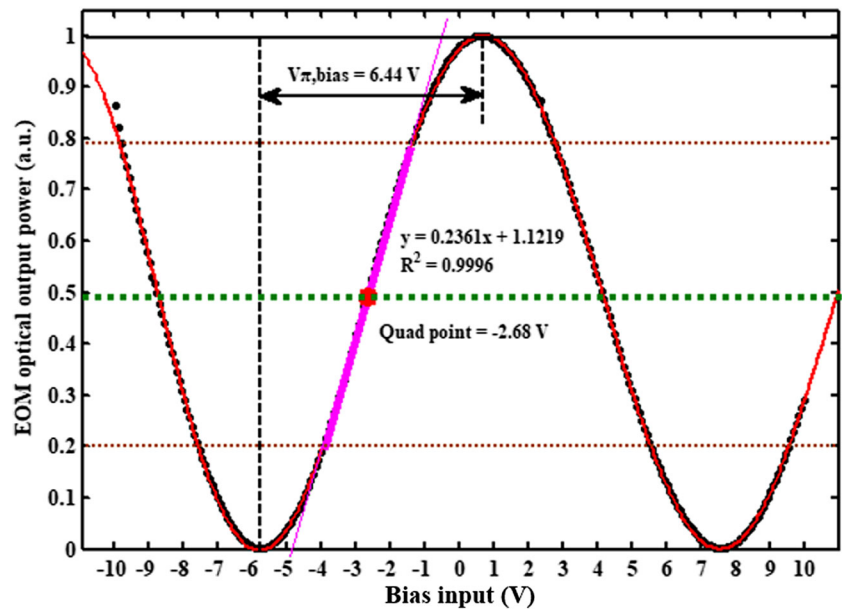


**Fig. 7** (Color online) Residual transmission value is measured by zooming in on bottom area of transmission curve

### 5 Measurement conditions

A 900- $\mu\text{m}$  semi-tight tube fiber type is used for the EOM pigtail, and the thermal coefficient of delay (TCD) of the 900- $\mu\text{m}$  semi-tight tube is 55 fs/m/K [23, 24]. According to the working principle of the BAM, it is necessary to evaluate the temperature stability of the transit time delay of the fiber length at the EOM input. Consider the fiber length at the EOM input as a total fiber length of 1.5 m. The transit time delay per unit of temperature change for the total fiber length of 1.5 m is then 82.5 fs/K. Therefore, in order to achieve a high BAM resolution, an active temperature stability control

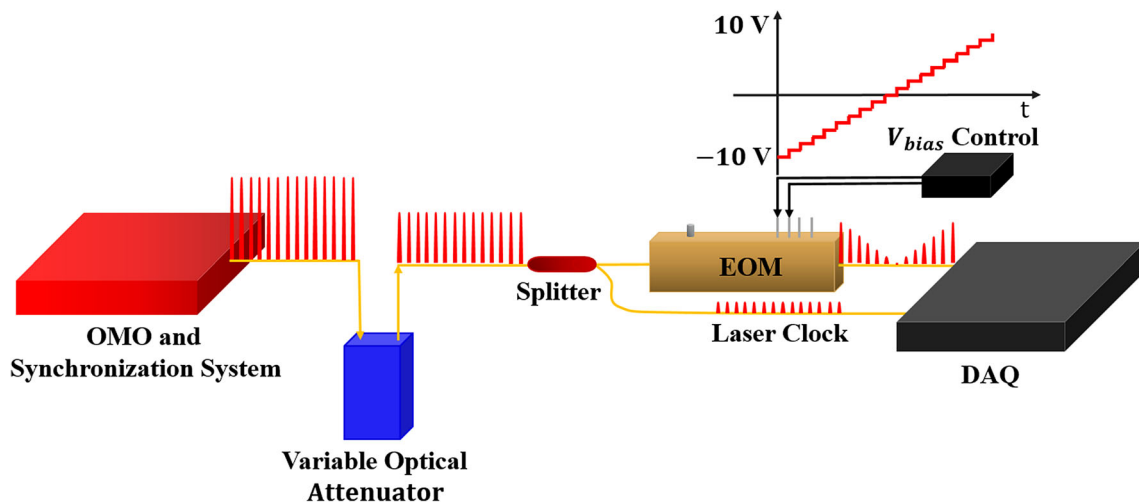


**Fig. 8** (Color online) Test platform based on DAQ system

**Fig. 9** (Color online) Principle block diagram of DAQ system

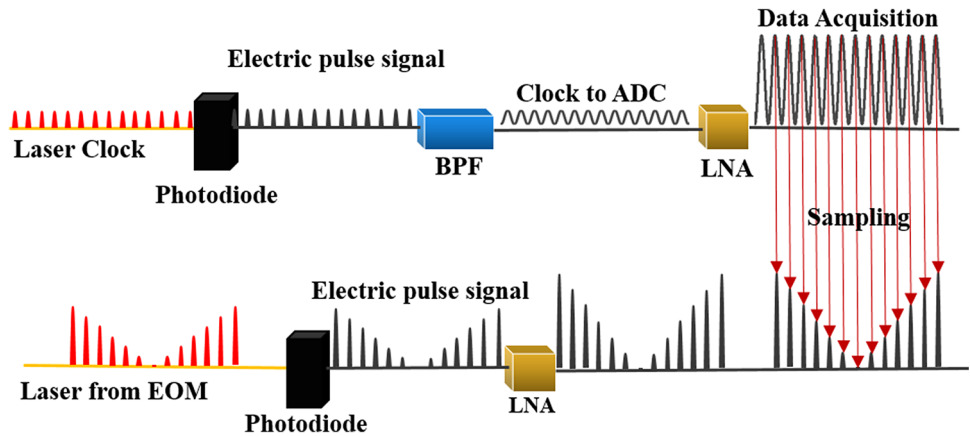


**Fig. 10** (Color online) Based on DAQ system test platform  $V_{\pi,bias}$ , Quad point voltage and linearity of a linear region  $R^2$  can be measured and calculated

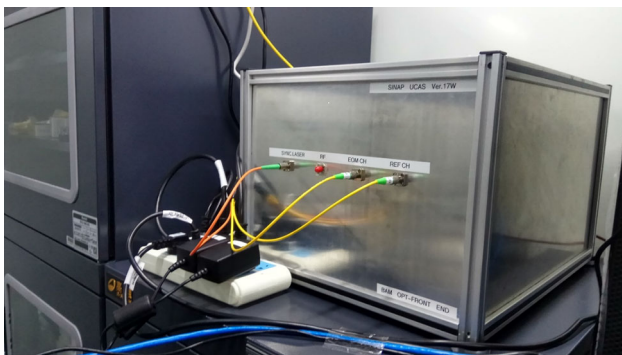
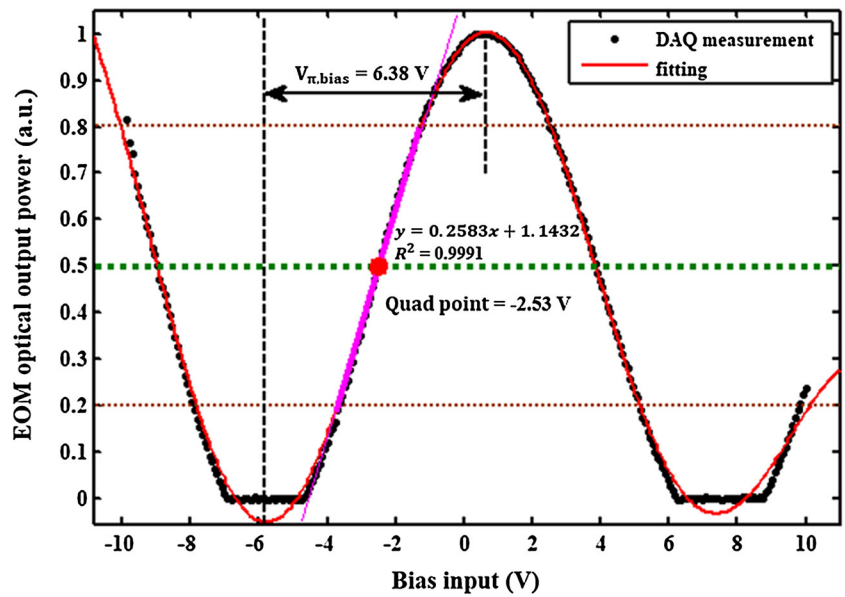


**Fig. 11** (Color online) Photograph of thermostat box for EOM testing

must be introduced. As shown in Fig. 11, the EOM was placed in a thermostat box for active constant temperature control.

In the thermostat box, an aluminum plate used to place the EOM is temperature stabilized to 5.5 mK (rms) over 1 h (Fig. 12) and 89 mK (rms) over a week (Fig. 13). Based on the temperature control performance of the aluminum plate placed in the thermostat box, the EOM input fiber introduces a temperature drift of 0.45 fs (rms) owing to temperature changes. Therefore, the temperature drift caused by temperature changes on the final resolution of the BAM is negligible. To ensure that the EOM performance test environment is similar to the actual operating environment, the two EOM comparison schemes mentioned above are measured under this constant temperature environment.

**Fig. 12** Temperature stability control performance of thermostat box over 1 h

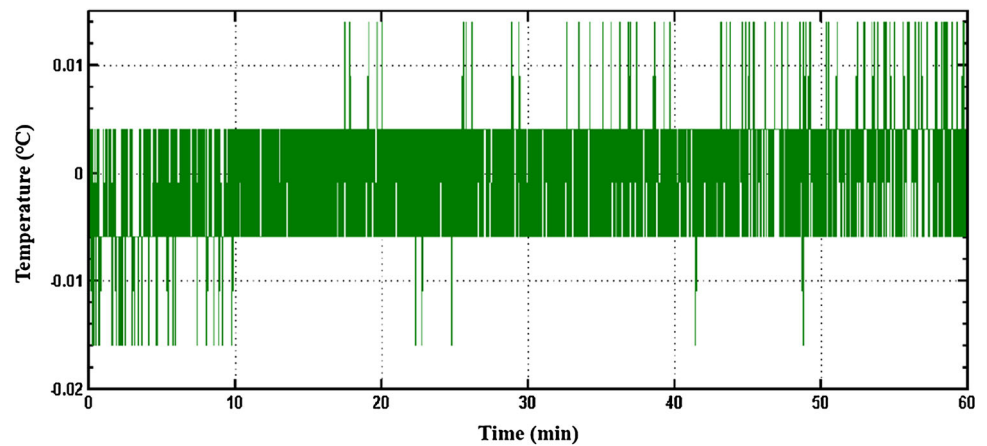
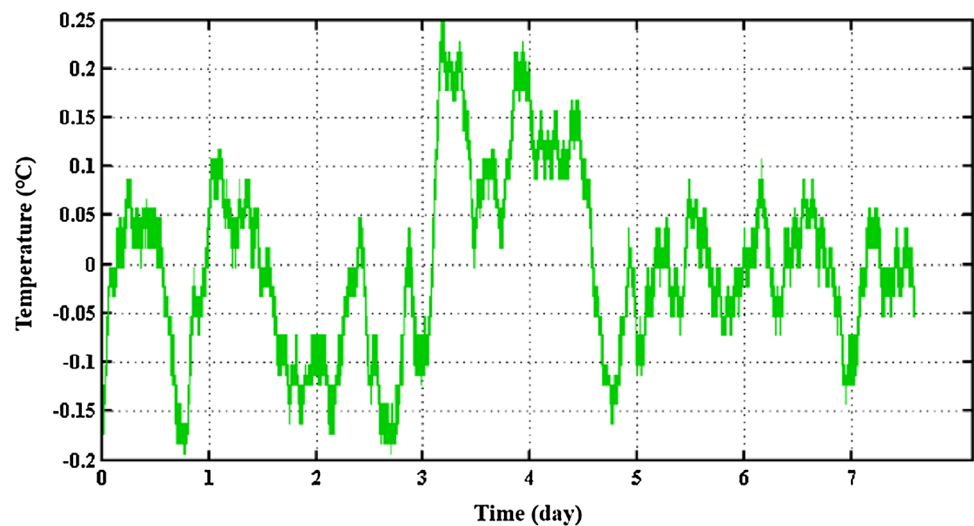


**Fig. 13** Temperature stability control performance of thermostat box over a week



## 6 Conclusion

The EOM serves as the core of the electro-optical modulation front end. It is essential for carrying out a detailed analysis of an EOM. From the EOM aspect, a higher measurement resolution of a new version of the BAM system requires a lower half-wave voltage  $V_{\pi,RF}$ , a higher modulation depth, and a higher bandwidth. In this paper, two different test platforms were designed to test the EOM for laser pulse modulation transmission curves. According to the measured EOM transmission curves, it can be known that the measured values of the two schemes have only a small difference that is negligible. The half-wave voltages of 6.44 V and 6.38 V were relatively high. This can be used for optimization in selecting the next version of EOM. The high linearity of the transmission

curve from 20 to 80% at 0.9996 and 0.9991, respectively, ensures the high sensitivity of the BAM.

The two schemes are analyzed by comparison. On the one hand, both test schemes identified that this type of electro-optical intensity modulator applied in the field of telecommunications also has high performance for laser pulse signals. On the other hand, the test platform based on the DAQ system is more reliable and flexible. Compared with the poor real-time performance and tedious operation of the optical power meter-based test platform, the DAQ system-based test platform can modify the environmental changes in real time.

In addition, the readout electronics is also part of the BAM system. However, because the ADC board only supports AC input, some distortion is observed when the electrical signal is weak. Therefore, it is necessary to make

certain improvements in the ADC board and introduce a DC bias voltage to the baseline. Alternatively, the peak and baseline of the electrical pulse signal can be sampled separately by dual ADCs and subtracted to obtain the true signal amplitude.

## References

1. J.M.J. Madey, Stimulated emission of bremsstrahlung in a periodic magnetic field. *J. Appl. Phys.* **42**, 1906 (1971). <https://doi.org/10.1063/1.1660466>
2. B.W.J. McNeil, N.R. Thompson, X-ray free-electron lasers. *Nat. Photonics* **4**, 814–821 (2010). <https://doi.org/10.1038/nphoton.2010.239>
3. P. Emma, R. Akre, J. Arthur et al., First lasing and operation of an Ångström-wavelength free-electron laser. *Nat. Photonics* **4**(9), 641 (2010). <https://doi.org/10.1038/nphoton.2010.176>
4. Z.T. Zhao, C. Feng, K.Q. Zhang, Two-stage EEHG for coherent hard X-ray generation based on a superconducting linac. *Nucl. Sci. Tech.* **28**, 117 (2017). <https://doi.org/10.1007/s41365-017-0258-z>
5. Z. Wang, C. Feng, Q. Gu et al., Generation of double pulses at the Shanghai soft X-ray free electron laser facility. *Nucl. Sci. Tech.* **28**, 28 (2017). <https://doi.org/10.1007/s41365-017-0188-9>
6. W.Y. Zhang, Q.X. Liu, L. Feng et al., 2.856 GHz microwave signal extraction from mode-locked Er-fiber lasers with sub-100 femtosecond timing jitter. *Nucl. Sci. Tech.* **29**, 91 (2018). <https://doi.org/10.1007/s41365-018-0419-8>
7. P.G. O'Shea, H.P. Freund, Free-electron lasers: status and applications. *Science* **292**(5523), 1853–1858 (2001). <https://doi.org/10.1126/science.1055718>
8. U. Bergmann, J. Corlett, S. Dierker et al., Science and Technology of Future Light Sources. A white paper, ANL-08/39, 2008. <https://doi.org/10.2172/948040>
9. L.H. Yu, Generation of intense UV radiation by subharmonically seeded single-pass free-electron lasers. *Phys. Rev. A* **44**, 5178. (1991). <https://doi.org/10.1103/physreva.44.5178>
10. L.H. Yu, M. Babzien, I. Ben-Zvi et al., First lasing of a high-gain harmonic generation free-electron laser experiment. *Nucl. Instrum. Methods A* **445**, 301–306. (2000). [https://doi.org/10.1016/S0168-9002\(00\)00131-5](https://doi.org/10.1016/S0168-9002(00)00131-5)
11. L.H. Yu, M. Babzien, I. Ben-Zvi et al., High-gain harmonic-generation free-electron laser. *Science* **289**, 932–934 (2000). <https://doi.org/10.1126/science.289.5481.932>
12. G. Stupakov, Using the Beam-echo effect for generation of short-wavelength radiation. *Phys. Rev. Lett.* **102**, 074801 (2009). <https://doi.org/10.1103/physrevlett.102.074801>
13. D. Xiang, G. Stupakov, Echo-enabled harmonic generation free electron laser. *Phys. Rev. ST Accel. Beams* **12**, 030702 (2009). <https://doi.org/10.1103/physrevstab.12.030702>
14. Z.T. Zhao, D. Wang, J.H. Chen et al., First lasing of an echo-enabled harmonic generation free-electron laser. *Nat. Photonics* **6**, 360–363 (2012). <https://doi.org/10.1038/nphoton.2012.105>
15. Shanghai Soft X-ray FEL (SXFEL), Conceptual Design Report (2015)
16. F. Loehl, K. Hacker, H. Schlarb, WEPB15: A sub-50 femtosecond bunch arrival time monitor system for FLASH, in *Proceedings of DIPAC*, Venice, Italy, 20–23 May 2007
17. F. Löhl, V. Arsov, M. Felber et al., Electron bunch timing with femtosecond precision in a superconducting free-electron laser. *Phys. Rev. Lett.* **104**, 144801 (2010). <https://doi.org/10.1103/physrevlett.104.144801>
18. J.G. Wang, B. Liu, THPML065: Preliminary results of the bunch arrival-time monitor at SXFEL, in *Proceedings of IPAC*, Vancouver, Canada, April 29 to May 4, 2018. <https://doi.org/10.18429/jacow-ipac2018-thpml065>
19. R.G. Hunsperger, *Integrated Optics Theory and Technology*, 6th edn. (Springer, New York, 2009), pp. 117–188
20. M.K. Bock, Measuring the Electron Bunch Timing with fs Resolution at FLASH. Ph.D. thesis, University Hamburg, Hamburg, Germany (2013)
21. A. Kuhl, S. Schnepp, A. Angelovski et al., MOPD34: Analysis of new pickup designs for the FLASH and XFEL bunch arrival time monitor system, in *Proceedings of DIPAC*, Hamburg, Germany, 16–18 May (2011)
22. Photline MXAN-LN series datasheet. [https://photonics.ixblue.com/files/files/pdf/Modulators/MX-LN\\_SERIES.pdf](https://photonics.ixblue.com/files/files/pdf/Modulators/MX-LN_SERIES.pdf)
23. L.A. Bergman, S.T. Eng, A.R. Johnston, Temperature stability of transit time delay for a single-mode fibre in a loose tube cable. *Electron. Lett.* **19**(21), 865–866 (1983). <https://doi.org/10.1049/el:19830587>
24. M. Bousonville, M.K. Bock, M. Felber et al., MOPG033: New phase stable optical fiber, in *Proceedings of BIW2012*, Newport News, VA USA. 15–19 April (2012)